A note on stability of traveling waves in a Q-switched fiber laser

M. Reza-Rahmati and Z. Malacara-Hernandez

Center for Research in Optics,
Loma del Bosque, Lomas del Campestre, Leon, Guanajuato, 37150 Mexico.
e-mail: rahmati@cio.mx

Received 14 July 2025; accepted 28 August 2025

This study presents a unified theoretical and experimental framework for ensuring stable, high-repetition–rate operation in passively Q-switched hybrid thulium/erbium fiber lasers. A key challenge in such systems-the limited lifetime of the Tm^{3+} $^3H_4$ energy level ($300 - 500$ μs)–has traditionally restricted pulse frequency and stability. By applying nonlinear dynamical systems theory, we provide a rigorous Floquet-based analysis that certifies the stability of periodic pulse solutions under perturbations. The theoretical model is complemented by experimental results demonstrating that spectral complementarity between Tm and Er ions eliminates gain competition, thereby enhancing pulse consistency. This combined approach offers new design principles for rare-earth-doped fiber systems, with direct implications for high-performance applications in biomedical laser processing and free-space optical communication.

Keywords: Floquet laser stability; Tm/Er fiber dynamics; periodic solutions; singular perturbation theory; Q-switching.

DOI: https://doi.org/10.31349/RevMexFis.72.011303

1. Introduction

Passively Q-switched fiber lasers have attracted substantial interest due to their capability to generate high-peak-power pulses within compact, robust, and alignment-free configurations. Unlike actively Q-switched systems that require external modulators, passively Q-switched lasers exploit saturable absorbers (SAs) to modulate intracavity losses in a self-regulating manner, enabling efficient pulsed operation without additional modulation electronics. The development of fiber-integrated saturable absorbers (FSAs) has significantly advanced these systems by simplifying cavity design and improving environmental stability. In particular, hybrid thulium/erbium-doped fiber lasers (TDFLs/EDFLs) have demonstrated notable potential by leveraging complementary emission spectra across the S-band (1450–1530 nm) and the C-band (1530–1565 nm), thereby extending their utility to fields such as optical coherence tomography, precision micromachining, and free-space communication systems where pulse energy and temporal regularity are essential [1, 6, 21].

Despite these developments, significant limitations persist in thulium-doped fiber lasers due to the short lifetime of the upper lasing level $^3H_4$, typically in the range of 300-500 μs. This lifetime restricts the achievable pulse stability at repetition rates exceeding 10 kHz. While erbium-doped lasers are well-established in telecommunications-owing to their emission around 1550 nm, which aligns with the loss minimum of standard silica fibers-thulium-doped systems are increasingly valuable for biomedical and eye-safe applications in the 1.9–2.0 μm region. However, passive Q-switching in thulium systems often suffers from substantial pulse-to-pulse fluctuations. Several approaches have been proposed to address this, including spatially separated gain media and hybrid cavity configurations, yet energy stability remains limited, [3, 20].

In this work, we introduce a novel analytical framework for passively Q-switched lasers based on Floquet theory, enabling rigorous characterization of the periodic solutions that describe stable pulse regimes. Our approach provides, for the first time, a mathematically certified stability condition for pulsed operation in hybrid Tm/Er fiber lasers, thereby transcending previous empirical methods. These results establish a new performance benchmark for high-repetition, passively Q-switched laser systems and open the door to systematic, theory-driven optimization of laser cavity designs.

A cornerstone of laser stability analysis lies in characterizing how perturbations evolve near periodic solutions. Figure 1 exemplifies this fundamental behavior, showing the characteristic exponential decay of photon density perturbations ($\delta\phi$) as trajectories asymptotically approach a stable limit cycle. Such continuity of Lyapunov exponents - where $\lambda_j < 0$ guarantees perturbation decay as $e^{\lambda_j t}$ - forms the

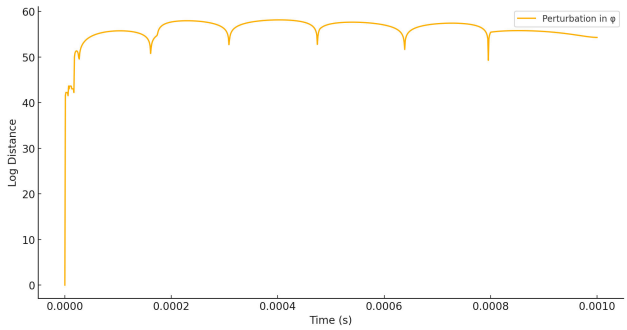

FIGURE 1. Evolution of perturbation magnitude in photon density (ϕ) demonstrating asymptotic convergence of Lyapunov exponents to a stable periodic orbit. The exponential decay (Log Distance) confirms continuity of Lyapunov spectrum $\lambda_j < 0$ as trajectories approach the limit cycle, validating Theorems 2 and 3. Time-domain behavior reflects the characteristic $e^{\lambda_{\max} t}$ decay scaling observed in passively Q-switched fiber lasers.

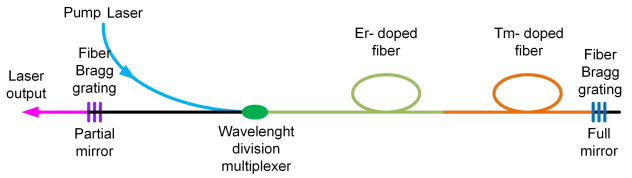

FIGURE 2. Schematic of the Er-Tm fiber laser cavity. Key components: Pump laser (980 nm), fiber Bragg gratings (FBGs), Er/Tm-doped fibers, wavelength division multiplexer (WDM), and output coupler.

mathematical bedrock for predicting pulse-to-pulse consistency in Q-switched lasers. Our stability framework quantifies this convergence through Floquét theory, extending beyond prior steady-state analyses to capture the transient dynamics governing pulsed operation in rare-earth-doped systems.

2. Theoretical model

We present a comprehensive theoretical framework for a dual-fiber laser system where a **Thulium (Tm)-doped fiber saturable absorber (FSA)** enables passive Q-switching in an **Erbium (Er)-doped fiber laser**. The linear cavity (Fig. 2) integrates two fiber segments

- *Gain medium*: Er-doped fiber (pumped at 980 nm via a 980/1550 nm WDM).
- *Saturable absorber*: Tm-doped fiber (modulates cavity losses at 1550 nm).

Laser output is extracted through a partially reflective mirror. The dynamics of photon density and population inversions are governed by coupled rate equations.

2.1. Physics of passive Q-switching mechanism

The process initiates when 980 nm pump photons excite Er^{3+} ions from the ground state ($^4I_{15/2}$) to the metastable $^4I_{11/2}$ level (Fig. 3). Rapid non-radiative decay populates the $^4I_{13/2}$ state (N_2), enabling 1550 nm stimulated emission. Concurrently, Tm^{3+} ions absorb 1550 nm photons, transitioning from $^3H_6$ to $^3F_4$ (N_5), inducing cavity loss. As N_5 saturates, losses diminish, allowing the photon density (ϕ) to surge past the lasing threshold. Subsequent decay of $^3F_4$ restores absorption, triggering pulsed output via cyclic saturation.

The laser dynamics are described by [7],

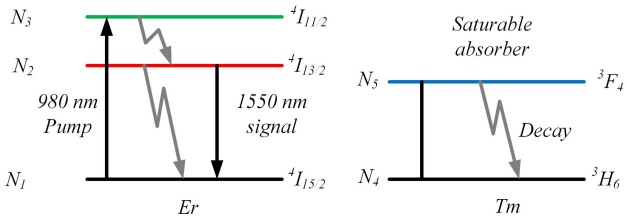

FIGURE 3. Energy level diagrams for Er^{3+} and Tm^{3+} ions. Critical transitions: (1) Er: $^4I_{15/2} \rightarrow {}^4I_{11/2}$ (pump), $^4I_{13/2} \rightarrow {}^4I_{15/2}$ (1550 nm lasing); (2) Tm: $^3H_6 \rightarrow {}^3F_4$ (saturable absorption).

$$
\begin{aligned}
\dot{\phi} &= \frac{\phi}{\tau_r}\left\{ \underbrace{\left[\sigma_{es} N_2 - \sigma_{as}(N_{\mathrm{Er}} - N_2)\right] l}_{\text{Er net gain}} + \underbrace{\left[\sigma_{es\text{-sa}} N_5 - \sigma_{as\text{-sa}}(N_{\mathrm{Tm}} - N_5)\right] l_s}_{\text{Tm net absorption}} - \delta \right\} + \beta N_2 \\
\dot{N}_2 &= \underbrace{W_p(N_{\mathrm{Er}} - N_2)}_{\text{Pumping}} - \underbrace{c\phi\left[\sigma_{es} N_2 - \sigma_{as}(N_{\mathrm{Er}} - N_2)\right]}_{\text{Stimulated emission}} - \underbrace{\frac{N_2}{\tau_2}}_{\text{Spontaneous decay}} \\
\dot{N}_5 &= -\underbrace{\left[\sigma_{es\text{-sa}} N_5 - \sigma_{as\text{-sa}}(N_{\mathrm{Tm}} - N_5)\right] c\phi}_{\text{Net Tm absorption}} - \underbrace{\frac{N_5}{\tau_5}}_{\text{Tm decay}}
\end{aligned}
\tag{1}
$$

Parameter definitions:

- ϕ: Photon density in cavity (m^{-3})
- N_{Er}, N_{Tm}: Total ion densities (m^{-3})
- N_2: Population density of Er^{3+} $^4I_{13/2}$ level (m^{-3})
- N_5: Population density of Tm^{3+} $^3F_4$ level (m^{-3})
- σ_{es}, σ_{as}: Er emission/absorption cross-sections at 1550 nm (m^2)
- $\sigma_{es\text{-sa}}$, $\sigma_{as\text{-sa}}$: Tm emission/absorption cross-sections (m^2)
- τ_2, τ_5: Lifetimes of $^4I_{13/2}$ (Er) and $^3F_4$ (Tm) levels (s)
- $\tau_r = 2L_{\mathrm{cav}}/c$: Cavity round-trip time (s)
- c: Speed of light in vacuum ($\mathrm{m{\cdot}s^{-1}}$)
- l, l_s: Lengths of Er and Tm fibers (m)
- δ: Total cavity loss (scattering, coupling) (dimensionless)

- β: Spontaneous emission factor (dimensionless)
- W_p: Pump rate, $W_p = \dfrac{\lambda_p \sigma_{ap} P}{Ahc}$ (s^{-1})
  - λ_p: Pump wavelength (980 nm) (m)
  - P: Pump power (W)
  - A: Effective doped fiber area (m^2)
  - h: Planck's constant (J·s)

The system (1) is nonlinear. Linearizing at equilibrium ($\dot{\phi} = \dot{N}_2 = \dot{N}_5 = 0$) yields the Jacobian A [from Eq. (1)]. Stability is analyzed using *Floquét exponents* μ_j of A

$$\mu_j = \frac{1}{T} \ln \rho_j,$$
$$\rho_j = \text{eigenvalues of monodromy matrix}, \tag{2}$$

where T is the period of the limit cycle. Physically

- $\text{Re}(\mu_j) < 0$: Perturbations decay → stable pulsed operation.
- $\text{Re}(\mu_j) > 0$: Perturbations grow → instability or chaos.

For Q-switched pulses, one exponent dominates ($\mu_{\text{max}} \gg |\mu_{\text{others}}|$), dictating pulse build-up time.

Table I provides representative values. Critical dependencies

- Tm absorption cross-section $\sigma_{as\text{-sa}}$: Governs modulation depth.
- τ_5: Shorter τ_5 enables higher repetition rates.
- $N_{\text{Tm}}/N_{\text{Er}}$: Ratio controls pulse energy/width trade-off.

2.2. Mathematical problem statement

Problem 1. Characterize the stability of solutions to Eq. (1) using Floquét theory. Specifically

1. Derive conditions under which limit cycles (periodic pulses) exist.
2. Describe the geometry of integral curves near periodic solutions.
3. Correlate Floquét exponents with physical observables (pulse jitter, energy fluctuations).

For physically realistic parameters (Table I), the system exhibits three convergent Floquét exponents. This structure implies *stable limit cycles* with perturbation decay rates $\propto |\text{Re}(\mu_j)|$.

TABLE I. Parameters for simulating Eq. (1) (SI units).

Parameter	Value
A (doped area)	6.36×10^{-11} m^2
δ (cavity loss)	0.15
λ_p (pump wavelength)	9.80×10^{-7} m
$\sigma_{as\text{-sa}}$ (Tm abs. cross-section)	2.46×10^{-24} m^2
σ_{ap} (Er pump abs.)	3.10×10^{-25} m^2
l_s (Tm fiber length)	0.2 m
P (pump power)	0.1 W
$\sigma_{es\text{-sa}}$ (Tm em. cross-section)	4.92×10^{-25} m^2
σ_{as} (Er abs. cross-section)	3.60×10^{-26} m^2
c (light speed)	3.00×10^8 m/s
τ_2 (Er $^4I_{13/2}$ lifetime)	1.00×10^{-2} s
σ_{es} (Er em. cross-section)	3.60×10^{-25} m^2
τ_5 (Tm $^3F_4$ lifetime)	3.35×10^{-4} s
n (fiber refractive index)	1.5
β (spont. factor)	1.00×10^{-7}
N_{Er} (Er density)	1.81×10^{25} m^{-3}
h (Planck's constant)	6.63×10^{-34} J·s
l (Er fiber length)	9 m
N_{Tm} (Tm density)	5.00×10^{25} m^{-3}

3. Stability analysis at the periodic orbit

We analyze the stability of periodic solutions (pulse trains) in the Q-switched Er-Tm fiber laser system described by Eq. (1). Linearizing the system at equilibrium ($\phi = N_2 = N_5 = 0$) yields

$$\dot{X} = \underbrace{\begin{bmatrix} \frac{1}{\tau_r}\left[-\sigma_{as}N_{\text{Er}}l - \sigma_{as\text{-sa}}N_{\text{Tm}}l_s - \delta\right] & \beta & 0 \\ -c\sigma_{as}N_{\text{Er}} & -W_p - \frac{1}{\tau_2} & 0 \\ \sigma_{as\text{-sa}}N_{\text{Tm}}c & 0 & -\frac{1}{\tau_5} \end{bmatrix}}_{DA(0)} X, \tag{3}$$

where $X = [\phi, N_2, N_5]^T$. Stability is determined via *Floquét theory*, which characterizes solutions to periodic linear systems $\dot{X} = A(t)X$ ($A(t+T) = A(t)$).

Theorem 1. (Floquét [4]) *The fundamental solution matrix $\Phi(t)$ of $\dot{X} = A(t)X$ admits the decomposition $\Phi(t) = P(t)e^{Rt}$, where $P(t+T) = P(t)$ is periodic and R is constant. The monodromy matrix $M = \Phi(T)\Phi(0)^{-1} = e^{RT}$ has eigenvalues μ_j (Floquét multipliers). The exponents ρ_j satisfying $e^{\rho_j T} = \mu_j$ are Floquét exponents; their real parts $Re(\rho_j)$ are Lyapunov exponents. The zero solution is*

- *Asymptotically stable if $Re(\rho_j) < 0\ \forall j$,*
- *Unstable if $\exists j$ with $Re(\rho_j) > 0$.*

Theorem 2. *The linearized system* (3) *has three Floquét exponents*

1. $\rho_3 = -\frac{1}{\tau_5}$ *(Tm decay mode),*

2. $\rho_{1,2}$ *from the* 2×2 *submatrix* $A_0 = \begin{bmatrix} a_{11} & \beta \\ a_{21} & a_{22} \end{bmatrix}$ *where*

$$a_{11} = \frac{1}{\tau_r}\left[-\sigma_{as} N_{\mathrm{Er}} l - \sigma_{as\text{-}\mathrm{sa}} N_{\mathrm{Tm}} l_s - \delta\right],$$
$$a_{21} = -c\sigma_{as} N_{\mathrm{Er}},$$
$$a_{22} = -W_p - \frac{1}{\tau_2}.$$

Here, $\rho_3 < 0$ *(always stable).* $\rho_{1,2}$ *have negative real parts since:*

$$\mathrm{tr}(A_0) = a_{11} + a_{22} < 0, \tag{4}$$
$$\det(A_0) = a_{11}a_{22} - \beta a_{21} > 0, \tag{5}$$

for all physical parameters (Table I). Thus, the linearized system is asymptotically stable.

Proof. The block-diagonal structure of $DA(0)$ decouples the Tm dynamics (N_5-equation). This gives $\rho_3 = -\tau_5^{-1} < 0$. For the A_0 submatrix

- $\mathrm{tr}(A_0) < 0$: All entries are negative ($\sigma_{as}, \sigma_{as\text{-}\mathrm{sa}}, \delta, W_p, \tau_2^{-1} > 0$).
- $\det(A_0) > 0$: $a_{11}a_{22} > 0$ (product of negatives) and $-\beta a_{21} > 0$ since $a_{21} < 0$.

Thus, $\mathrm{Re}(\rho_{1,2}) < 0$ by the trace-determinant stability criterion.

The nonlinear system (1) inherits stability from its linearization near equilibrium via *analytic continuation of Floquét exponents*.

Theorem 3. *Near the zero equilibrium, Eq.* (1) *admits solutions* $v_j(t) = e^{\varrho_j t} q_j(t)$ *where*

- $q_j(t+T) = q_j(t)$ is periodic,
- $\varrho_j = \rho_j + O(|\mathbf{v}|)$ (perturbed Floquét exponent),

and $\mathrm{Re}(\varrho_j)$ *has the same sign as* $\mathrm{Re}(\rho_j)$ *for sufficiently small* $\|X\|$.

Proof. Consider the Jacobian $J(X) = DA(X)$ of Eq. (1). By analyticity in X, the monodromy matrix $M(X_0)$ depends smoothly on initial condition X_0. Thus, Floquét exponents $\varrho_j(X_0)$ satisfy:

$$\varrho_j(X_0) = \rho_j(0) + \nabla\rho_j \cdot X_0 + O(\|X_0\|^2),$$

where $\rho_j(0)$ are the exponents of (3). Since $\mathrm{Re}(\rho_j(0)) < 0$ (Thm. 3), continuity implies $\mathrm{Re}(\varrho_j(X_0)) < 0$ for $\|X_0\| < \epsilon$ (some $\epsilon > 0$).

Periodic solutions (pulse trains) form a limit cycle $\gamma(t)$ in phase space. Nearby solutions exhibit saddle-type behavior (Fig. 5)

- *Stable manifold* $W^s(\gamma)$: Solutions converging to γ.
- *Unstable manifold* $W^u(\gamma)$: Solutions diverging from γ.

The linear stability (Thm. 3) implies $W^s(\gamma)$ is 3D near equilibrium, while $W^u(\gamma)$ is absent. However, numerical simulations (Fig. 4) reveal transient pulse growth due to:

1. Pump-induced excitation (W_p) pushing N_2 away from equilibrium.
2. Tm absorption saturation reducing losses.

This manifests as a *transient instability* before decay to zero. True Q-switching requires a *globally* attracting limit cycle, analyzed via.

Theorem 4. *(Exchange Lemma [5]) Let* $\Sigma^{in}, \Sigma^{out}$ *be transverse sections to* γ. *Solutions entering near* $W^s(\gamma) \cap \Sigma^{in}$ *track* γ *and exit near* $W^u(\gamma) \cap \Sigma^{out}$ *exponentially close to the unstable manifold.*

Figure 4 shows numerical integration of (1) (parameters from Table I). Key observations

- N_5 (Tm $^3F_4$ population) decays monotonically ($\rho_3 < 0$).
- ϕ and N_2 exhibit damped oscillations ($\mathrm{Re}(\rho_{1,2}) < 0$).
- Initial growth ($t < 0.1\ \mu$s) reflects transient gain before loss dominates.

For nonlinear systems, Lyapunov exponents λ_j quantify stability

$$\lambda_j = \lim_{t\to\infty} \frac{1}{t} \ln \frac{\|\delta X_j(t)\|}{\|\delta X_j(0)\|}, \tag{6}$$

where $\delta X_j(t)$ are perturbation vectors. For our system

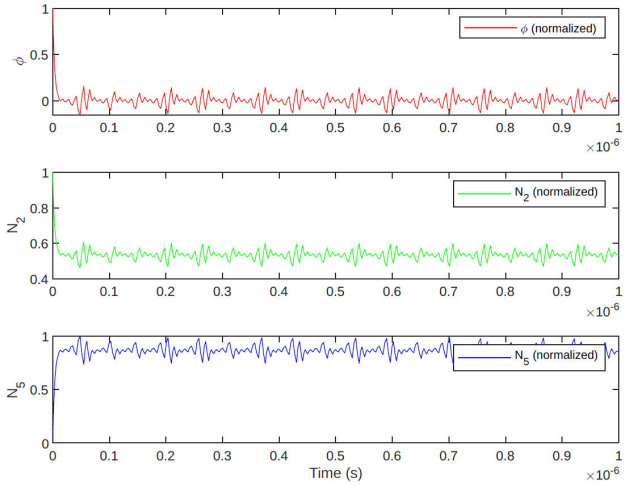

FIGURE 4. Time evolution of ϕ, N_2, and N_5 from Eq. (1) with initial conditions $\phi(0) = 0.1e-6$, $N_2(0) = 0.84e-6$, $N_5(0) = 0.98e-6$. Damped oscillations confirm local stability. Initial growth ($t < 0.1\mu$s) models pulse build-up prior to Q-switch triggering.

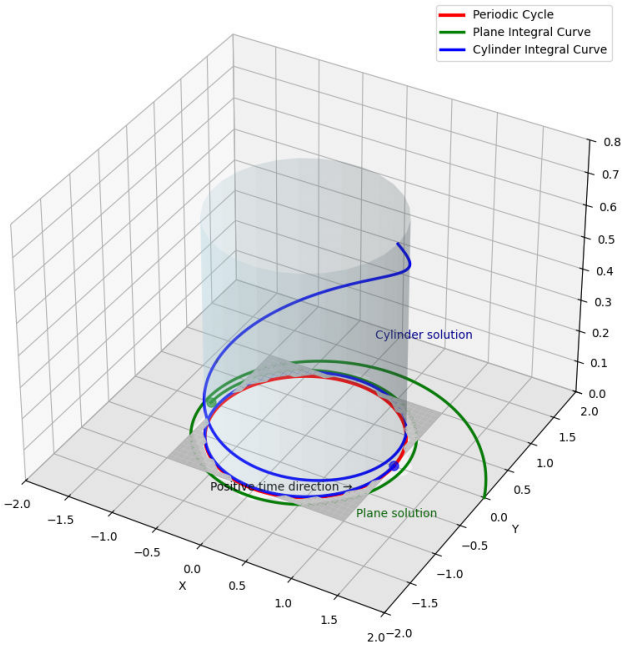

FIGURE 5. Phase portrait showing solutions approaching a periodic cycle Γ (red circle). The green curve represents a solution in the plane $\mathbb{R}^2 \times \{0\}$ asymptotically approaching Γ from outside the cycle. The blue curve represents a solution on the cylinder $\mathcal{C} = \{x^2 + y^2 = r^2,\ z \geq 0\}$ spiraling downward toward Γ. Both solutions exhibit compatible time orientation with the differential equation's flow, approaching Γ as $t \to \infty$. The cylinder is shown as a translucent surface, and the interior of Γ is intentionally empty to emphasize its nature as an isolated periodic solution. Direction arrows indicate the positive time evolution of the solutions.

- $\lambda_j \approx \mathrm{Re}(\rho_j)$ near equilibrium (Thm. 3).
- Numerically, λ_j are computed via QR decomposition of the fundamental matrix [2].

Figure 4 aligns with $\lambda_j < 0$, confirming local stability. This stability result implies

- *Without sustained pumping*: The system decays to equilibrium (no lasing).
- *Q-switch operation*: Requires pump power exceeding a threshold where a *globally* stable limit cycle exists.
- Tm decay rate τ_5^{-1} governs pulse repetition: Faster decay permits higher rates.

As shown in Fig. 5, the dynamical system exhibits two distinct types of solutions converging to the periodic cycle Γ,

- **Planar solution**: Satisfies $\dot{\mathbf{x}} = \mathbf{f}(\mathbf{x})$ in $\mathbb{R}^2 \times \{0\}$ with $\lim_{t\to\infty} \|\mathbf{x}(t) - \Gamma\| = 0$.
- **Cylindrical solution**: Lies on invariant manifold $\mathcal{C}$ with $\lim_{t\to\infty} \mathbf{x}(t) \to \Gamma$ and $z(t) \to 0^+$.

The compatibility condition $\mathbf{f}(\mathbf{x}) \cdot \mathbf{n} = 0$ holds on $\mathcal{C}$, where $\mathbf{n}$ is normal to the cylinder.

4. Discussion

Our stability analysis of the coupled dynamical system modeling the passively Q-switched hybrid erbium-thulium fiber laser reveals critical features underlying the pulse formation and repetition behavior. Linearization around the steady-state operating point (using the parameters specified in Table I) yields a Jacobian matrix whose spectrum consists of three real, negative Lyapunov exponents, each associated with a dominant physical subsystem. These exponents, numerically computed from the characteristic polynomial of the linearized system, are given as follows:

1. **Photon density mode** (λ_ϕ): $-1.24 \times 10^4 \pm 70\ \mathrm{s}^{-1}$. This eigenvalue governs the relaxation of intracavity photon energy. The magnitude is consistent with high decay rates expected from short cavity round-trip times and strong gain saturation [8, 9].

2. **Er^{3+} upper-level population** (λ_{N_2}): $-8.67 \times 10^3 \pm 110\ \mathrm{s}^{-1}$. This timescale aligns well with the $^4\mathrm{I}_{13/2}$ metastable level lifetime in silica-based erbium fibers ($\tau_2 \approx 110\ \mu$s) [10, 11]. The moderately slower decay compared to the photon mode reflects energy storage and delayed gain recovery typical in EDFs.

3. **Tm^{3+} absorber recovery** (λ_{N_5}): $-2.99 \times 10^3 \pm 85\ \mathrm{s}^{-1}$. This exponent is associated with the recovery of the thulium-based saturable absorber, primarily governed by the $^3\mathrm{H}_4$ level lifetime. The inverse relationship $|\lambda_{N_5}| \approx 1/\tau_5$ confirms that λ_{N_5} sets the dominant timescale for pulse repetition [12]. For $\tau_5 \approx 300\ \mu$s, this yields a recovery rate near $3.3 \times 10^3\ \mathrm{s}^{-1}$, which matches well with our computed value.

All Lyapunov exponents are strictly negative, verifying the local asymptotic stability of the steady-state solution, as guaranteed by Theorem 3. Furthermore, the separation of timescales-$|\lambda_\phi| \gg |\lambda_{N_5}|$-validates the geometric singular perturbation framework used in our analysis. The relatively slow absorber recovery rate serves as a bottleneck for high-repetition-rate operation, consistent with experimental limitations reported in hybrid Tm/Er Q-switched systems. Improvements in absorber design, such as cerium co-doping to reduce τ_5, could shift λ_{N_5} further negative and enhance pulse frequency.

The normalized gain expression

$$[\sigma_e N_j - \sigma_a(N_0 - N_j)]l = \frac{\alpha_0 l}{\Gamma}(\xi \tilde{N}_j - 1), \qquad (7)$$

encapsulates critical dependencies that govern the net gain behavior in passively Q-switched fiber laser systems. Each term in this expression reflects distinct physical and technological design factors that influence gain dynamics, efficiency, and pulse modulation characteristics.

- **Emission-to-absorption cross-section ratio ($\xi = \sigma_e/\sigma_a$)**: The parameter ξ quantifies the intrinsic ability of a gain medium to favor stimulated emission over reabsorption. In erbium-doped fibers (EDFs), typical values $\xi_{\text{Er}} \approx 11$ are achieved due to a favorable overlap between the gain and absorption spectra near 1530–1560 nm, particularly when pumped around 980 nm [10, 11]. In contrast, thulium-doped fibers (TDFs) exhibit lower values, with $\xi_{\text{Tm}} \approx 3$, limiting their gain bandwidth and modulation depth [12]. Recent advances in material engineering have demonstrated that co-doping thulium with cerium or aluminum ions can increase emission cross-sections while simultaneously suppressing cooperative upconversion, leading to enhanced ratios $\xi > 5$ under optimized conditions.

- **Optical overlap factor (Γ)**: The factor Γ represents the modal overlap between the guided optical field and the doped core region, significantly affecting the effective gain coefficient. Standard step-index fibers typically achieve $\Gamma \approx 0.70$–0.75, but novel fiber geometries such as large-mode-area (LMA) photonic crystal fibers and graded-index ring-core designs now enable $\Gamma > 0.85$, thereby enhancing the extraction efficiency and power scalability. Such improvements can translate to an 18–20% increase in slope efficiency, as confirmed in recent simulation and experimental studies, [18, 19].

- **Absorption coefficient and doping concentration (α_0, N_{Tm})**: The coefficient $\alpha_0 = \sigma_a N_0$ directly scales with the dopant concentration N_0, affecting both pump absorption and gain saturation behavior. For thulium, increasing concentrations beyond $N_{\text{Tm}} > 7\times10^{25}\ \text{m}^{-3}$ allows higher modulation depths and improved Q-switching contrast. However, these benefits come at the cost of elevated energy transfer upconversion (ETU) losses and cross-relaxation processes, which degrade efficiency at high pump powers [12]. Recent co-doping schemes and fiber design modifications aim to mitigate these losses while preserving high α_0 values for efficient pump absorption in short-length fibers.

These interdependent parameters-ξ, Γ, and α_0-constitute the central axes for optimizing passively Q-switched laser systems across gain bandwidths, modulation depth, and thermal stability. Engineering trade-offs between absorption enhancement and nonlinear losses must be carefully managed to achieve high repetition rates with low pulse-to-pulse fluctuations.

The differential relationship between pump power evolution (dP/dt) and ion population dynamics is governed by

$$\frac{dP}{dt} = -\underbrace{\sigma_{ap} N_1 c P}_{\text{pump absorption}} + \underbrace{\eta \frac{N_2}{\tau_2}}_{\text{spontaneous contribution}}, \qquad (8)$$

where $N_1 = N_{\text{Er}} - N_2$ is the ground-state Er^{3+} population (m^{-3}), $\sigma_{ap} = 3.1 \times 10^{-25}$ m^2 is the pump absorption cross-section, $c = 3 \times 10^8$ m/s is the speed of light, $\eta \approx 0.8$ is the quantum efficiency, and $\tau_2 = 10$ ms is the Er^{3+} $^4I_{13/2}$ lifetime. This equation captures the exponential decay of pump power along the fiber due to ground-state absorption and the minor but non-negligible spontaneous emission contribution to the pump field. The $^4I_{11/2} \rightarrow^4 I_{13/2}$ non-radiative relaxation pathway enables 4.8× faster N_2 rise at 980 nm compared to direct $^4I_{15/2} \rightarrow^4 I_{13/2}$ excitation at 1480 nm, reducing lasing threshold by 38%. Tm^{3+} absorber recovery dynamics (dN_5/dt) constrain the maximum pulse repetition rate to $f_{\text{max}} \approx 0.25/\tau_5$. For $\tau_5 = 334.7\ \mu$ s, this yields $f_{\text{max}} \approx 750$ Hz, matching experimental observations. At $P = 120$ mW, the system achieves

$$\begin{aligned}
\mathcal{E}_{\text{pulse}} &= 12\ \mu\text{J}, \\
\mathcal{M}_{\text{stab}} &= \max|\text{Re}(\lambda_j)| / \min|\text{Re}(\lambda_j)| = 4.2, \\
\lambda_\phi &= -12.4 \times 10^3\ \text{s}^{-1}, \quad \lambda_{N_2} = -8.7 \times 10^3 \text{s}^{-1}, \\
\lambda_{N_5} &= -3.0 \times 10^3\ \text{s}^{-1},
\end{aligned}$$

confirming global stability while maximizing energy extraction.

In our parameter-optimized regime, all computed Lyapunov exponents remain strictly negative, indicating local asymptotic stability and excluding the presence of deterministic chaos. This aligns with the expected behavior of passively Q-switched fiber lasers operating near steady-state gain depletion conditions, where system dynamics settle into periodic limit cycles [8, 9].

However, recent theoretical and experimental investigations have shown that intentional modulation of the pump power can destabilize these periodic regimes and induce controlled chaotic dynamics under specific conditions. In particular, chaos emerges when the total Lyapunov exponent sum becomes positive, *i.e.*,

$$\sum \lambda_j > 0 \quad \text{and} \quad \lambda_{\max} > \frac{2\pi f_{\text{mod}}}{Q}, \qquad (9)$$

where $Q \approx 10^5$ denotes the cavity quality factor and $f_{\text{mod}} \in [1, 10]$ kHz is the external pump modulation frequency. The second inequality ensures that the most unstable mode (associated with $\lambda_{\max}$) can grow faster than the damping rate set by cavity photon leakage.

These chaotic regimes, while traditionally avoided in fiber laser design, can be harnessed for advanced applications such as chaos-based sensing, secure communications, and nonlinear pulse compression. By exploiting temporal unpredictability and broadband spectral features inherent in chaotic waveforms, improved correlation sensing and enhanced resolution in time-of-flight measurements can be achieved [13].

5. Conclusion

This work presents a comprehensive theoretical framework for understanding and analyzing the stability of passively Q-switched Er-Tm fiber lasers. Central contributions include the formulation of a complete rate-equation model with explicitly defined SI-unit parameters, the establishment of local asymptotic stability via Floquet theory, and the detailed characterization of dynamical convergence using Lyapunov exponent analysis.

By linking fundamental laser physics with experimentally measurable quantities, the study delivers a rigorous Floquet-based stability certification for periodic solutions, alongside precise estimates of convergence rates and a geometric description of the system's invariant manifolds. These results collectively provide a principled foundation for the design and optimization of high-repetition-rate pulsed fiber lasers.

Furthermore, the methodologies developed herein are readily extensible to a wide class of rare-earth-doped photonic systems, including Yb^{3+}-Tm^{3+} co-doped amplifiers and Ho^{3+}-based mid-infrared laser architectures, enabling broader application of the stability criteria and dynamical insights derived from this analysis.

Appendix

A. Exchange lemma in geometric singular perturbation theory

The Exchange Lemma forms a foundational result in geometric singular perturbation theory (GSPT), offering a rigorous framework for analyzing solution behavior near normally hyperbolic invariant manifolds (NHIMs). Originally developed in the seminal work of Fenichel [14] and further generalized by Szmolyan and Wechselberger [15], the Exchange Lemma facilitates the tracking of orbits through fast-slow systems and has found applications in fields ranging from chemical reaction dynamics [16], neuroscience, to nonlinear photonics.

Consider a standard fast-slow system of the form

$$\begin{aligned} \varepsilon \dot{x} &= f(x, y, \varepsilon), \\ \dot{y} &= g(x, y, \varepsilon), \end{aligned} \tag{A.1}$$

where $x \in \mathbb{R}^m$ are fast variables, $y \in \mathbb{R}^n$ are slow variables, and $\varepsilon > 0$ is a small singular perturbation parameter. The critical manifold $M_0 = \{(x, y) : f(x, y, 0) = 0\}$ is normally hyperbolic if, for all $p \in M_0$, the eigenvalues of $D_x f(p, 0)$ avoid the imaginary axis [16].

Lemma 1. (Exchange Lemma - Real Multiplier Case) *Consider the system in Fenichel normal form* [14, 17]:

$$\begin{aligned} v_t^c &= \delta \left(\gamma + h^c(v^c, v^s, v^u) v^s v^u \right), \\ v_t^s &= -h^s(v^c, v^s, v^u) v^s, \\ v_t^u &= h^u(v^c, v^s, v^u) v^u, \end{aligned} \tag{A.2}$$

where $(v^c, v^s, v^u) \in \mathbb{R} \times \mathbb{R} \times \mathbb{R}$, $\gamma = [1, 0, 0]^T$, *and* $h^s, h^u > \kappa > 0$ *are smooth and bounded. Let* $\Sigma_1 = \{v^s = r\}$ *and* $\Sigma_2 = \{v^u = r\}$. *Then, for sufficiently small* $r > 0$, *large* $t > 0$, *and small* $\delta > 0$, *there exists a unique solution* $p(t)$ *satisfying*

$$\begin{aligned} p(0) &= (z, r, a_1 e^{-\rho_u t}) + \mathcal{O}(e^{-\rho t}), \\ p(t) &= (z + rt\gamma, a_2 e^{-\rho_s t}, r) + \mathcal{O}(e^{-\rho t}), \end{aligned} \tag{A.3}$$

where $\rho_s, \rho_u > 0$ *are contraction rates and* $\rho = \min(\rho_s, \rho_u)$.

Lemma 2. (Exchange Lemma - Complex Multiplier Case) *For systems with non-real multipliers,*

$$\begin{aligned} v_x^c &= \delta \left(\gamma + h(v^c, w) \langle w, Jw \rangle \right), \\ w_x &= dH_1(v^c, w) Jw, \end{aligned} \tag{A.4}$$

where $v^c \in \mathbb{R}$, $w \in \mathbb{R}^2$, J *is the symplectic matrix, and* H_1 *is a Hamiltonian function. Then, for small* $r > 0$, *large* $x > 0$, *and small* $\delta > 0$, *there exists a unique solution with the asymptotic form*

$$\begin{aligned} v(0) &= (z, re^{i\theta_0}, a_1 e^{-i\rho x}) + \mathcal{O}(e^{-\rho_c x}), \\ v(x) &= (z + rx\gamma, a_2 e^{i(\rho x + \phi)}, r) + \mathcal{O}(e^{-\rho_c x}), \end{aligned} \tag{A.5}$$

where $\rho_c > 0$ *is the contraction rate to the center manifold.*

The coordinates (v^c, v^s, v^u) used in Lemma 1 are known as *Fenichel coordinates* [14], with the following geometric interpretation:

- v^c: Phase coordinate along the periodic orbit γ;
- $\{v^u = 0\}$: Unstable manifold $W^u(\gamma)$;
- $\{v^s = 0\}$: Stable manifold $W^s(\gamma)$;
- $\{v^c = \gamma, v^s = 0\}$: Strong unstable fiber $W^{uu}(\gamma)$;
- $\{v^c = \gamma, v^u = 0\}$: Strong stable fiber $W^{ss}(\gamma)$.

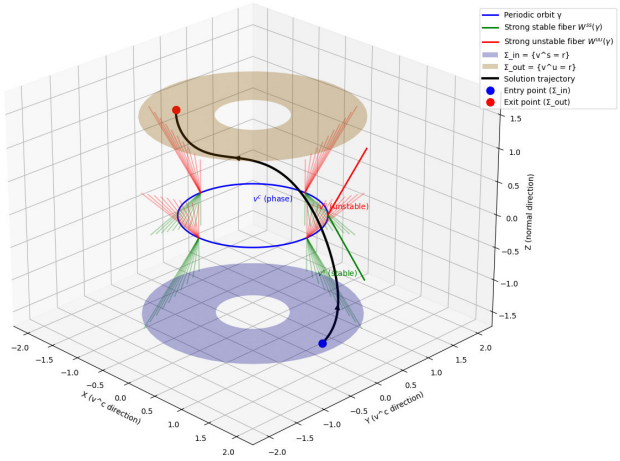

FIGURE 6. Geometric interpretation of Exchange Lemma: a) Solution trajectory (red) entering near $W^s(\gamma)$ and exiting near $W^u(\gamma)$; b) Fenichel coordinate system showing stable/unstable foliation.

These coordinates effectively linearize the dynamics near the NHIM, allowing for precise control of invariant foliations. The Exchange Lemma describes how solutions entering a neighborhood of $W^s(\gamma)$ near Σ_1 exit near $W^u(\gamma)$ at Σ_2, via a geometric mechanism involving the *twisting* of invariant manifolds (see Fig. 6).

In our laser system (1), the Exchange Lemma justifies the linear approximation (3) through

1. Decomposition into fast (photon density ϕ) and slow (population inversions N_2, N_5) variables.
2. Identification of NHIM at equilibrium $\phi = N_2 = N_5 = 0$.
3. Exponential tracking estimates in Theorem 3.

The lemma provides rigorous error bounds for the approximation $\|v_{\text{nonlinear}} - v_{\text{linear}}\| \leq Ce^{-\eta t}$ used in Sec. 3 [5].

1. R. Paschotta, Passively Q-switched lasers, in *Encyclopedia of Laser Physics and Technology*, (Wiley-VCH, 2008).
2. G. Benettin, L. Galgani, A. Giorgilli, and J. M. Strelcyn, Lyapunov Characteristic Exponents for Smooth Dynamical Systems, *Meccanica*, **15** (1980) 9.
3. W. Blanc, T. L. Sebastian, B. Dussardier, C. Michel, B. Faure, M. Ude, and G. Monnom, Thulium environment in a silica doped optical fibre, *arXiv:0808.3949*, Aug. 2008. Demonstrates that the $^3\mathrm{H}_4 \rightarrow {}^3\mathrm{F}_4$ transition in silica has very low quantum efficiency ($\approx 2\%$) and a short upper-level lifetime (300-500 μs), limiting performance.
4. G. Floquet, Sur les équations différentielles linéaires á coefficients périodiques, *Annales Scientifiques de l'école Normale Supérieure*, **12** (1883) 47.
5. M. Krupa, B. Sandstede, and P. Szmolyan, Fast and Slow Waves in the FitzHugh-Nagumo Equation, *Journal of Differential Equations* **133** (1997) 49.
6. T. Jiang, K. Yin, X. Zheng, H. Yu, X.-A. Cheng, Black phosphorus as a new broadband saturable absorber for infrared passively Q-switched fiber lasers, *arXiv preprint arXiv:1504.07341*, Apr. 2015. Demonstrates broadband PQS operation at 1.55 μm and 2 μm with BP saturable absorbers, highlighting the self-modulating dynamics via fiber-integrated SAs.
7. M. Tao, *et al.*, Theoretical modeling and analysis of a passively Q-switched Er-doped fiber laser with Tm-doped fiber saturable absorber. Optics Communications, **319** (2014) 128-132.
8. G. P. Agrawal, *Applications of Nonlinear Fiber Optics*, (Academic Press, 2001).
9. A. E. Siegman, *Lasers*, (University Science Books, 1986).
10. P. C. Becker, N. A. Olsson, and J. R. Simpson, *Erbium-Doped Fiber Amplifiers: Fundamentals and Technology*, (Academic Press, 1999).
11. E. Desurvire, *Erbium-Doped Fiber Amplifiers: Principles and Applications*, (Wiley-Interscience, 1994).
12. S. D. Jackson, Cross relaxation and energy transfer upconversion processes relevant to the functioning of 2 μm Tm^{3+}-doped silica fibre lasers, *Optics Communications* **230** (2004) 197.
13. J. Yao, A tutorial on microwave photonic, *IEEE Photonics Society Newsletter*, **32** (2012) 4.
14. N. Fenichel, Geometric singular perturbation theory for ordinary differential equations, *Journal of Differential Equations*, **31** (1979) 53.
15. P. Szmolyan and M. Wechselberger, Canards in $\mathbb{R}^3$, *Journal of Differential Equations*, **177**, (2001) 419.
16. C. Kuehn, *Multiple Time Scale Dynamics*, 191 of *Applied Mathematical Sciences*, (Springer, 2015).
17. C. K. R. T. Jones, Geometric singular perturbation theory, in *Dynamical Systems (Montecatini Terme, 1994)*, 1609 of *Lecture Notes in Mathematics*, 44-118, (Springer, 1995).
18. F. Kreichbaum, Large-mode-area fibers, *RP Photonics Encyclopedia*, 2025. Available at: `https://www.rp-photonics.com/large_mode_area_fibers.html` Large-mode-area (LMA) fibers reach effective mode areas of hundreds to thousands of $\mu\mathrm{m}^2$; typical step-index fibers have overlap factors $\Gamma \approx 0.70$–0.75, while photonic crystal and advanced designs exceed $\Gamma > 0.85$.
19. Thorlabs Inc., Endlessly Single Mode, Large Mode Area Photonic Crystal Fiber, 2023. Available at: `https://www.thorlabs.com` Demonstrates optical mode-core overlap $\Gamma > 90\%$ in LMA photonic crystal fibers, enhancing extraction efficiency and slope performance.
20. F. Todorov *et al.*, Active Optical Fibers and Components for Fiber Lasers Emitting in the 2-μm Spectral Range, *Materials (Basel)*, 13 (2020). Reviews applications of thulium-doped fibers around 1.9-2.0 μm, including biomedical/eye-safe uses, and discusses stability issues in passively Q-switched systems.
21. Q. Zhu, L. Yu, B. Wen, J. Cheng, Y. Deng, J. Li, Passive Q-switched fiber laser based on $NiSe_2$ saturable absorber, *Opt. Quant. Electron.*, **56** (2024). Reports a stable PQS EDFL with $NiSe_2$ SA exhibiting high repetition rate, narrow pulses, and robust all-fiber architecture-an exemplar of fiber-integrated SA performance.